

Revealing a full quantum ladder by nonlinear spectroscopy

Darius Abramavicius^{1,*}

¹Institute of Chemical Physics, Physics Faculty, Vilnius University, Sauletekio 9-III, LT-10222 Vilnius Lithuania
*darius.abramavicius@ff.vu.lt

ABSTRACT

Coherent two-dimensional spectroscopy in IR or visible region is very effective for studying correlations, energy relaxation/transfer pathways in complex multi-chromophore or multi-mode systems. However it is usually restricted up to two-quanta excitations and their properties. In this paper an arbitrary level of excitation is suggested as the utility to scan nonlinear potential surfaces of quantum systems up to a desired excitation degree. This can be achieved by a simple three-pulse laser spectroscopy approach. Accurate evaluation of high-level anharmonicities as well as transition amplitudes can be directly obtained. Additionally, questions regarding the quantum nature of the probed system can be addressed by studying absolute peak positions.

Introduction

Impulsive laser spectroscopy is one of the main material science utilities for revealing excited states dynamics. The forefront in the nonlinear domain, the two-dimensional coherent spectroscopy (2DIR in IR region, 2DES in visible region)^{1,2}, which has been applied in solid^{3,4}, protein^{5,6}, liquid^{7,8} as well as gaseous⁹ materials. It has been also utilized in microscope configuration¹⁰. 2D spectroscopy evolved from of the transient absorption spectroscopy. The two-pulse pump probe or transient absorption approach provides the time resolution by measuring the transient evolution of difference absorption induced by the excitation pump pulse and the detection probe pulse. Since the two pulses provide the time resolution as the delay between pump and probe pulses, the measurement essentially reflects the change of induced response of the sample in time. By adding a third laser pulse in e. g. in a three pulse photon echo peak shift (3PEPS) approach, the additional time delay of intraband coherence allows to additionally follow the environment-induced correlation functions of the energy gap fluctuations¹¹⁻¹³. The pump probe and 3PEPS rely on the four wave mixing (4WM) process in the nonlinear system, however, from a theory point of view, the specific convolutions of the third order molecular response function are performed and detected in these approaches^{11,14}. The convolutions are lifted by ultrashort excitation pulses imitating elementary perturbative excitations. A natural upgrade to the 4WM techniques then results in four pulse setup when the full deconvoluted information contained in the third order response function is retrieved by the two-dimensional heterodyne detected coherent spectroscopy. Denoting i -th pulse wavevector by k_i , in this case, the specific component of the four wave mixing process can be associated with the system-field interaction configuration, and by collecting signals $-k_1 + k_2 + k_3$, $k_1 - k_2 + k_3$, $k_1 + k_2 - k_3$, all available information contained in the third order response function with largest possible time and frequency resolution can be gathered^{1,2}. Ideally since each excitation pulse provides a single (one quantum) excitation with a dedicated wave vector, the specific peaks in spectra can be associated with a minimal set of interaction pathways. The obtained two-dimensional (2D) spectrum sometimes is denoted as representing a picture of "quantum tomography"^{15,16}.

In the visible optical regime the 4WM measurements mainly demonstrate the properties of the single exciton manifold in $-k_1 + k_2 + k_3$ and $k_1 - k_2 + k_3$ configurations. The single excitation manifold is very important in physical chemistry as the single excitations are main players in excitation transport, charge separation, charge transport processes in molecular and biological functional systems¹⁷⁻²⁴.

The double excitation manifold, i. e. the set of states, which are achieved by sequential two photon absorption participate in excited state absorption in transient absorption, 3PEPS and 2DES. The double-exciton level structure or exciton-exciton correlation is directly achieved in $k_1 + k_2 - k_3$ (double quantum coherence) detection^{25,26} or in fifth order 2D spectra where exciton-exciton annihilation becomes considerable²⁷⁻³⁰.

While the dynamical aspects of energy migration is the main focus in electronic spectroscopy, the 2D spectroscopy approach in IR regime³¹ has been utilized for molecular structure determination^{2,32,33} and for tracking thermal fluctuations and chemical reaction dynamics³⁴⁻³⁷ via vibrational resonances. Vibrational nonlinear spectroscopy allows direct measurement of diagonal and off diagonal vibrational anharmonicities^{38,39}. These parameters are related to single and double quanta properties, hence,

denote the lowest order nonlinear properties of the complex vibrational potential surfaces^{40–42}. Several spectroscopic methods, including infrared and ultraviolet absorption, Raman, jet-cooled laser-induced fluorescence, have been utilized to map out the whole series of vibrational quantum states of molecules in their ground and excited electronic states^{43–45}. These multiple quanta properties are very important for numerous molecular processes such as chemical reactions^{46,47}, isomerization or inversion^{48–52}, as well as energy transfer during inelastic collisions proceed along vibrational pathways that are governed by vibrational potential energy surfaces^{53,54}. Development of spectroscopic approaches to reveal the whole vibrational (or electronic) potential surface is thus highly demanded and simple nonlinear spectroscopy probes can aid in this direction.

In this letter a set of nonlinear optical measurements is suggested to directly measure multiple-quanta up to a desired degree excitation properties. The obtained two-dimensional spectra then can be employed to reveal the energy level structure of a potential surface what is necessary for reconstruction of molecular potential surfaces. A side question regarding the quantum nature of vibrations can be addressed as well.

Theory and simulations

Optical excitations of a quantum system can be easily described by the response function theory at various orders with respect to the system-field interactions. Using a response function formalism the induced polarization's j -th order to the field component is given by

$$P^{(j)}(t) = \int_0^\infty dt_j \cdots \int_0^\infty dt_1 S^{(j)}(t_j \dots t_1) \times E(t-t_j)E(t-t_j-t_{j-1})\dots E(t-t_j-\dots t_1) \quad (1)$$

In an electric dipole approximation all even orders lead to vanishing response of bulk samples. We next consider a single color source excitation field with frequency resonant to one particular anharmonic molecular mode. Before hitting the sample, the field is split into a set of excitation fields

$$E(t) = \sum_i^N E_i(t) = \sum_i^N A_i(t) \exp(i\mathbf{k}_i \mathbf{r} - i\omega t) + c.c.$$

Here $A_i(t)$ is a slowly varying amplitude of the i -th component whose wavevector is \mathbf{k}_i . In nonlinear regime the phase matching phenomenon is an additional necessary companion in the optical spectroscopy. Indeed, multiplication of such fields in Eq. 1 results in superpositions of wavevectors, and thus the signals are being generated with the specific new signal wave vectors given by $\mathbf{k}_s = n_1 \mathbf{k}_1 + n_2 \mathbf{k}_2 + \dots n_N \mathbf{k}_N$. Here N is the number of incoming fields, n_1, \dots, n_N are integers each taking values in the interval $-j, -j+1 \dots j-1, j$, where j is the order of nonlinearity and we have additionally $|n_1| + |n_2| + \dots + |n_N| = j$.

Spatial detuning of laser rays can be used to reveal specific output wavevectors. The collinear geometry can be also used to increase the field overlap region and specific phase matched configuration can be obtained by phase cycling. Phase cycling for N incoming pulses is formally equivalent to the spatial Fourier transformation in N dimensions. To isolate an m -th order component ($m+1$ wave mixing) on a single dimension one needs to use at least $m+1$ equally distributed phase values as dictated by periodicity of Fourier transform and Nyquist theorem (see Fig. 1 a). Indeed the discrete transform of equally spaced M samples in x dimension of a function $f(x_i) = f_i$ yields M samples in conjugate k_x dimension. So for distinguishing ± 1 output values one needs to provide $M=4$ input distinct values corresponding to $-1\Delta_x, 0\Delta_x, +1\Delta_x, +2\Delta_x$ or $-1k_x, 0k_x, +1k_x, +2k_x$ samples. Notice that in $M=4$ case due to periodicity of Fourier transform $-2k_x \equiv +2k_x$ cannot be distinguished.

At first, we may consider designing a high order multidimensional spectroscopy to probe highly lying excited states and reveal complete nonlinear response function in the spirit of 2DES. Notice that at 3-rd order to the field by adding the third harmonic generation configuration, $k_s = k_1 + k_2 + k_3$, the number of independent phase matching components is $2^3/2 = 4$ (half of 2^3 components are conjugate to each other), at j -th order we thus have $2^j/2$. Hence, in order to gather the complete information available at j -th order, the number of phase matched configurations which have to be inspected scales exponentially with the order in the field.

Such “complete-information” way of thinking calls for an experiment where for j -th order we should consider j laser pulses. However, it becomes impossible to continue in this spirit as the dimensionality of the phase matching configurations and dimensionality of signal as a function of time delays, grows up and the amount of gathered data becomes prohibitively large.

Hence, as higher-energy and quanta states become populated in higher-order spectroscopies the focus of the problems must shift towards the multiple-excitation characteristics. The most important information then for example is the energy level configuration or in other words the shape of potential surface⁵⁵. It should be noted that this used to be the main focus of the 2DIR where vibrational anharmonicities have been resolved³¹.

Notice that high order nonlinear interaction process is not necessarily related to a large number of laser pulses. Indeed a single field induces response at an arbitrary order to the field and the phase matching unravels specific interaction pathways.

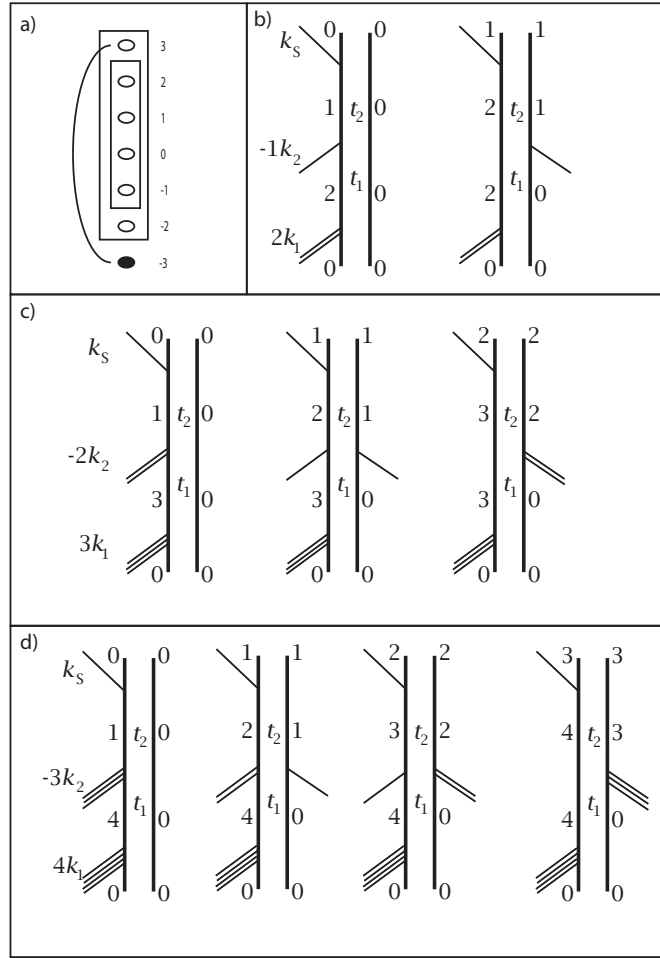


Figure 1. a) Resolution of wave vector components in phase matching process as viewed from spatial Fourier transform. Feynman diagrams for the $k_s = nk_1 - (n - 1)k_2$ phase matching configuration with two excitation pulses: b) at 3-rd ($n = 2$), c), at 5-th ($n = 3$), d) and at 7-th ($n = 4$) order to the field.

The ideal approach is to use a smallest number of excitation pulses to reveal the desired information on n -quanta energy levels. A sequential process may be designed by two pulses to drive the excitation up and down the ladder to the quantum states and then detect the optical coherence field.

Consider for example a response induced by two incoming laser pulses. The first pulse corresponds to wavevector k_1 while the second to k_2 . Let's inspect the induced polarization detected at $k_s = nk_1 - (n - 1)k_2$, where n is an arbitrary integer. The Feynman diagrams corresponding to such process are given in Figure 1b-d. In this setup, during the first delay interval t_1 the state of the system is given by coherent superposition of the ground state and the n -th excited state that is reached by absorption of n photons. In the case of small anharmonicity, the corresponding density matrix element oscillates with the frequency approximately equal to $n\omega_0$, where ω_0 is the frequency of the photon, provided anharmonicity is small. The following $n - 1$ interactions (either on the left or on the right of the diagram) with the second pulse after delay t_1 generate interband coherences that range from $|1\rangle\langle 0|$ to $|n\rangle\langle n - 1|$. The diagram thus projects information about $1, 2, \dots, n$ quanta excited states onto a two-dimensional function of delays t_1 and t_2 . The latter can be Fourier transformed into a two-dimensional spectrum $S(\omega_1, \omega_2)$.

Notice that considering n quanta excitations the strongest transitions are between $n \rightarrow n \pm 1$ levels; these transitions originate from a single light quantum absorption/emission. Hence, in $k_s = nk_1 - (n - 1)k_2$ configuration all involved transitions are of single quantum absorption/emission, so the signal intensity is never scaled by a small anharmonic correction of the transition dipole.

As an example the multiple quanta spectra of a Morse oscillator is presented in the following. The Morse oscillator is a unique anharmonic quantum system whose energy levels and transition amplitudes are available analytically⁵⁶. The potential

surface of the oscillator can be given by

$$V(x) = D(1 - \exp(-\alpha x))^2 \quad (2)$$

with D being the classical ionization energy, α is the curvature parameter of the potential valley. For the case when mass of the oscillator is $1/2$, the oscillator fundamental frequency is equal to $\omega_\alpha = 2\alpha\sqrt{D}$. By taking for convenience $\alpha = 1$ we find that D is the only anharmonicity parameter. Denoting $D = (\mathcal{N} + 1/2)^2$, the integer part of $\mathcal{N} + 1/2$ (which we denote by $N = \text{Int}[\mathcal{N} + 1/2]$) equals to the number of discrete quantum levels. Essentially the system is more anharmonic as the number of discrete energy levels gets smaller and the oscillator turns into harmonic system with $D \rightarrow \infty$. Energy spectrum of the discrete states of the oscillator in this case is

$$E_n = -(\mathcal{N} - n)^2 \quad (3)$$

with $n = 0, 1 \dots N - 1$. In the following we assume that the dissociation is not relevant and we do not consider the continuum part of the spectrum, since its contribution to the spectrum is quite weak (checked numerically, not shown).

The next required quantity is the optical transition dipole moment. In order to determine it, it is necessary to define the polarization operator. The polarization operator for a harmonic oscillator is often assumed to be proportional to the coordinate operator, $\hat{P} = \mu\hat{x}$. We next assume that the optical field only involves transitions between adjacent energy levels and other transitions are off resonant. We thus consider only matrix elements $\langle n|\hat{P}|n+1\rangle$ ⁵⁶:

$$\mu_n \equiv \mu \langle n|\hat{x}|n+1\rangle = \mu \frac{\sqrt{(\mathcal{N}-n)(\mathcal{N}-n-1)}}{\mathcal{N}-n-1/2} \left[\frac{(n+1)}{(2\mathcal{N}-n)} \right]^{\frac{1}{2}} \quad (4)$$

which for large $\mathcal{N} \gg n$ reduces to the result of a harmonic oscillator $\mu_{n+1}/\mu_n \approx \sqrt{(n+2)/(n+1)}$.

Consequently, we can write analytically the resulting expressions for the 2D peak intensities. For example for $k_s = 4k_1 - 3k_2$ we have the set of peaks whose amplitudes in the harmonic case are approximately equal to $4!\mu_0$ since the system in each diagram absorbs and emits up to 4 quanta. In general for the signal component $k_s = nk_1 - (n-1)k_2$ the peak intensities will be $n!\mu_0$.

All distinct diagrams have positions determined by resonant transition energies. The fundamental energy gap

$$\omega_0 = E_1 - E_0 = 2\mathcal{N} - 1, \quad (5)$$

and correspondingly the sequence of energy gaps

$$E_{n+1} - E_n = \omega_0 - 2n \quad (6)$$

is linear with n . This sequence is directly observed in $k_s = nk_1 - (n-1)k_2$ configuration.

By using the diagram approach we can easily show what peaks will be visible in 2D spectrum for various wavevector configurations for Morse oscillator. The oscillation frequency in the t_1 interval is

$$E_n - E_0 = n\omega_0 - \Delta_n \quad (7)$$

with $\Delta_n = n(n-1)$, so the sets of peaks in $k_s = nk_1 - (n-1)k_2$ measurement will appear at frequency $w_1 = n\omega_0 - \Delta_n$. During t_2 the system will oscillate with frequencies corresponding to energy gaps $E_{i+1} - E_i = \omega_0 - \Delta_{2i}$ for $i = 0, 1 \dots n$. Such situation is demonstrated on the top of Figure 2.

To demonstrate the above described approach in more realistic scenario, we next present numerical simulations of the excitation and detection process of the Morse oscillator with dephasing and lineshapes. We set the oscillator parameter $\mathcal{N} = 8$, so that the number of bound states is $N = 8$. The initial state of the system is equal to the ground state $|0\rangle$. For the excitation process, which we represent as action by nonlinear excitation operator, $X_\phi \rho_0$, we assume excitation by an optical field resonant to the fundamental frequency and with the bandwidth covering all transitions $n \rightarrow n+1$. In order to realize that the excitation/deexcitation is nonperturbative (as in real experiment) we numerically integrate the interaction picture Schrödinger equation with the excitation field turned on. For Liouville equation this results in iteration of equation

$$\dot{\rho} = -i(\mu_\phi \rho - \rho \mu_\phi), \quad (8)$$

here

$$\mu_\phi = A \begin{pmatrix} 0 & \mu_1 e^{-i\phi} & 0 & \dots & 0 \\ \mu_1 e^{i\phi} & 0 & \mu_2 e^{-i\phi} & \dots & 0 \\ 0 & \mu_2 e^{i\phi} & 0 & \dots & 0 \\ \dots & \dots & \dots & \dots & \dots \\ 0 & 0 & 0 & \dots & 0 \end{pmatrix} \quad (9)$$

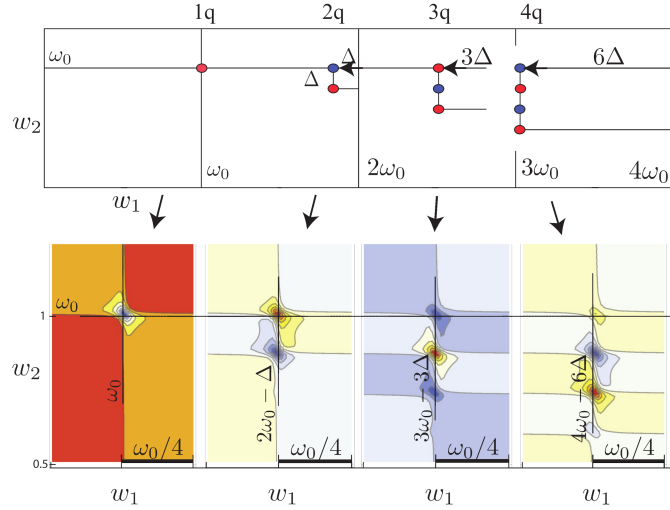


Figure 2. Top: scheme of peaks in the $k_S = nk_1 - (n-1)k_2$ measurement of Morse oscillator corresponding to (from left to right) $n = 1, n = 2, n = 3$ and $n = 4$. ω_0 is the fundamental frequency and Δ is the lowest anharmonicity. Bottom - the spectrum of the Morse oscillator obtained from solving Liouville equation and the signal (Eq. 11) is reconstructed by phase cycling. The damping is included as an additional factor to the signal as $\exp(-\gamma(t_1 + t_2))$ with $\gamma = 0.02\omega_0$ so that all resonances are explicitly expressed.

is the transition dipole operator with only RWA terms including the excitation intensity A and phase ϕ (the phase is necessary for phase cycling to recover correct phase matching contributions). This equation is propagated for an infinitesimal time interval $\delta t \rightarrow 0$ with the given intensity A , so that $A\delta t$ is not vanishing and can be tuned to populate the chosen number of states.

So the protocol is as follows. We take the initial density matrix

$$\rho_0 = \begin{pmatrix} 1 & 0 & \dots \\ 0 & 0 & \dots \\ \dots & \dots & \dots \end{pmatrix}, \quad (10)$$

perform excitation $X_{\phi_1}\rho_0$ with phase ϕ_1 , then we perform the density matrix propagation according to Liouville equation with the field switched off to obtain $\mathcal{G}(t_1)X_{\phi_1}\rho_0$. The second excitation follows with the phase ϕ_2 : $X_{\phi_2}\mathcal{G}(t_1)X_{\phi_1}\rho_0$, propagation with the field off for time delay t_2 : $\mathcal{G}(t_2)X_{\phi_2}\mathcal{G}(t_1)X_{\phi_1}\rho_0$, and finally we perform the final detection to obtain the signal

$$S(t_1, t_2) = \text{Tr}\{\mu_L \cdot \mathcal{G}(t_2)X_{\phi_2}\mathcal{G}(t_1)X_{\phi_1}\rho_0\}. \quad (11)$$

We emphasize the difference between this expression and standard response function theory, where each excitation event is a linear operation. In our approach we assume that each operation $X_{\phi_i}\rho$ is nonlinear and thus generates the whole spectrum of harmonics.

On the bottom of Fig. 2 we present a series of 2D spectra after Fourier transform $S(t_1, t_2) \rightarrow S(\omega_1, \omega_2)$ for the signal $k_S = nk_1 - (n-1)k_2$ with $n = 1, 2, 3, 4$ that correspond to the nonlinear signals at 1, 3, 5, 7 order. The line broadening was kept small.

The common critique to these types of simulations is that the line broadening has to be maintained small in order to observe the peak pattern and to determine the anharmonicity. However, in this type of signal that is not an issue because we observe not a single pair of peaks, but the whole train of peaks. The same simulations of 2D spectra with large line broadening ($\gamma = 0.1\omega_0$) is shown in Figure 3. On the top row we can observe that overlapping peaks become squeezed, but the number of peaks and peak splitting can be uniquely determined.

Additional question on the quantum nature of oscillations can be addressed in this case. We additionally show the corresponding classical simulation results, i.e. for the same type of Morse potential but obtained from purely classical equations of motion. We find that the peak pattern is quite similar, however its overall absolute position becomes shifted 2 the series of peaks becomes positioned symmetrically with respect to theoretical central point equal to $(\omega_2, \omega_1) = (\omega_0, n\omega_0)$, while the series is shifted in the case of quantum oscillator.

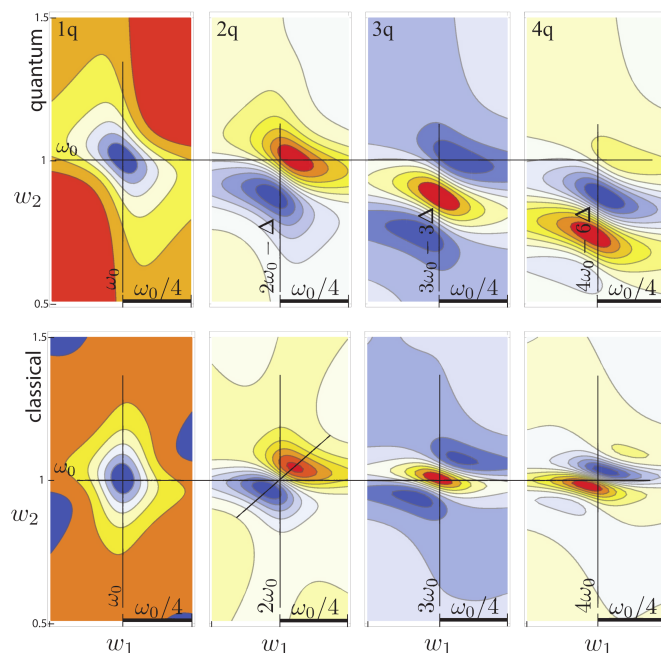


Figure 3. Numerical simulations of $k_S = nk_1 - (n - 1)k_2$ signals of Morse oscillator corresponding to (from left to right) $n = 1, n = 2, n = 3$ and $n = 4$ cases for the quantum (top) and classical (bottom) oscillators. ω_0 is the fundamental frequency and Δ is the lowest anharmonicity. Line broadening parameter is set to $\gamma = 0.1\omega_0$.

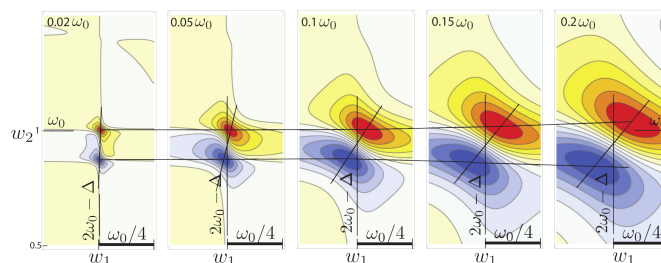


Figure 4. Numerical simulations of simple 2DIR signal of the Morse oscillator with the increasing linewidth parameter γ shown in insets of the subplots.

Discussion and conclusions

So where is the next level of impulsive spectroscopy? In this paper the direction towards higher order nonlinear interactions is considered. The fifth order coherent spectroscopy has been considered in IR and visible and the complex information on the correlations in quantum systems has been represented in 3DIR⁵⁷ or 3DES^{58–60} or 3D fluorescence⁶¹. By spreading frequencies into a third spectral dimension high frequency vibronic modes⁵⁸, double-exciton resonances^{27–29} or specific exciton relaxation pathways^{59,60} have been revealed. To collect the complete information, five excitation pulses are needed for generation of interaction pathway-specific detailed picture. The full set of information then comes up in five dimensions as five independent time intervals between interactions should be considered. Utilizing e. g. the gradient assisted photon echo (GRAPE) methodology, the fifth-order nonlinear polarization through three sequential single-quantum coherences have been measured in parallel⁵⁸ and presumably could be extended for 5D measurement. However, the information contents in the corresponding full-scale experiments becomes huge, and interpretation becomes challenging.

The approach presented in this paper is not related to extracting all possible information at a certain order, but, instead, is specifically geared to extract only small amount of information, but with a minimal amount of effort with high accuracy. A similar approach has been utilized to gain high-order electronic correlations in quantum wells⁶².

This specificity can be demonstrated with respect to the vibrational anharmonicity that is often targeted in 2DIR of proteins. Simple numerical simulations in Fig. 4 demonstrate that the anharmonicity that is being extracted from simple 2DIR measurement may be distorted by large broadening, and thus, cannot be used to accurately determine the corresponding

hamiltonian parameters. Meanwhile Fig. 3(top) demonstrates that the anharmonicity is revealed not only on vertical but also on horizontal axes and can be accessed without interference from line overlaps.

It should be noted that other anharmonic properties should be included when using more accurate simulation approaches. For example, 0-2, 0-3 etc. transition dipole elements of the Morse potential are not zero, additionally at high excitation levels, continuums states can be reached. On the spectroscopy side this could indicate an interesting turn for the spectroscopy analysis, while on the chemical side this can be used to initial chemical reactions or molecular isomerization.

The approach described in this paper in general applies not only to vibrational excitations but also to electronic states of molecules or atoms, but would require careful analysis of the spectra as electronic oscillators are highly anharmonic and positions of double-triple quanta excitations are poorly *a priori* anticipated (that may not be the case for Rydberg atoms in gas phase, etc.)

The other question that comes up is what kind of new information can be extracted from such multi-dimensional signals. In electronic time resolved spectroscopy the excitation relaxation pathways are primary targets and, for example, according to the perturbation theory the relaxation process depends on the two point fluctuation correlation function⁶³. In principle the n -th order nonlinear signal is dependent on the $n + 1$ point correlation function¹⁴. So 1-st order response (linear absorption) is related to the two-point correlation function $C(t_2, t_1)$ which reduces to $C(t_2 - t_1)$ due to the assumption of ergodicity (equilibrium before the measurement), and is in principle sufficient to reveal the relaxation phenomena. Indeed the dephasing and relaxation processes determined spectral lineshape positions and broadening. The correlation function here is considered in a broad sense to include also the electronic degrees of freedom. The third order response function maps the four-point correlation functions. The electronic degrees of freedom (i. e. energy level structure) become reflected onto the 2D plot in two-dimensional coherent spectroscopy, while the vibrational part of the correlation function results in spectral lineshapes. However, assuming the fluctuation process as a Gaussian process, all multi-point correlation functions split into a set of simple two-point, $C(t_i - t_j)$, correlation functions. Consequently, going to higher orders does not necessarily generate novel information. Recently at fifth order to the field the exciton-exciton annihilation processes have been considered that encapsulate the novel four particle correlation properties as they originate from $\hat{a}^\dagger \hat{a}^\dagger \hat{a} \hat{a}$ terms²⁷⁻²⁹, however, focusing on exciton migration again restricts the focus again only to the one-particle diffusion problem.

The level of complexity becomes overwhelming in biological systems where interactions between electronic and vibrational degrees of freedom may have important implications for rapid and efficient energy transfer. Development of higher-order spectroscopies that may enable unambiguous assignment of signals to specific pathways is very active. Highly nonlinear Raman approaches have been proposed since 2000⁶⁴. 2D Resonance Raman techniques denoted by femtosecond Stimulated Raman Spectroscopy (FSRS), yield a subset of the quantum pathways⁶⁵⁻⁶⁷ reveal electronic and vibrational interactions, however, suffer from contributions from cascades of third-order processes⁶⁸⁻⁷⁰. Direct correlation between impulsively driven low-frequency modes such as phonons, vibrations and (multi-)excitons with quantum coherence selectivity through control of resonance can specifically be probed by fifth order gradient-assisted multidimensional electronic Raman spectroscopy (GAMERS) free from low order cascades⁷¹. Hence, target-specific approaches are advantageous.

It should be noted that large field intensities are often necessary to reach good signal to noise ratio at high nonlinearity orders. Then high order nonlinearities become involved in apparent low degree phase matching configurations that are supposed to be sensitive only to low orders to the field. For example the traditional photon echo $k_s = -k_1 + k_2 + k_3$ configuration may be plagued by other superpositions, like $k_s = -k_1 - k_1 + k_1 + k_2 + k_3$, etc., which come from the fifth order^{27,29}. Similarly, seventh, ninth and so on orders contribute to the specific phase matching configuration. Therefore studying high-order nonlinearities in seemingly low order phase matching configurations, e. g. exciton annihilation in pump-probe, carries large nonzero background. Instead in our suggested approach we have a zero background signal, what allows to cleanly identify the specific order without "poisoning" by higher orders when lowest possible excitation intensity is maintained. Alternatively, low order cascading signals may obscure the highly nonlinear signals in simple phase matching configurations. Approach suggested in this paper could be free from cascading contributions if spatial phase matching in non-collinear laser configuration is applied. In collinear scheme with phase matching the error control must be very high level to avoid cascading.

Concluding, a simple two-excitation-pulse nonlinear spectroscopy approach is proposed to reveal quantum ladder of states in an anharmonic oscillator. Consequently this could be employed in reconstruction of whole potential surface at a desired excitation level.

References

1. Abramavicius, D., Palmieri, B., Voronine, D. V., Šanda, F. & Mukamel, S. Coherent multidimensional optical spectroscopy of excitons in molecular aggregates; quasiparticle versus supermolecule perspectives. *Chem. Rev.* **109**, 2350–2408, DOI: [10.1021/cr800268n](https://doi.org/10.1021/cr800268n) (2009).

2. Zhuang, W., Hayashi, T. & Mukamel, S. Coherent multidimensional vibrational spectroscopy of biomolecules: Concepts, simulations, and challenges. *Angew. Chemie - Int. Ed.* **48**, 3750–3781, DOI: [10.1002/anie.200802644](https://doi.org/10.1002/anie.200802644) (2009).
3. Cho, M. *Two-Dimensional Optical Spectroscopy* (CRC Press, 2009).
4. Wen, P., Christmann, G., Baumberg, J. J. & Nelson, K. A. Influence of multi-exciton correlations on nonlinear polariton dynamics in semiconductor microcavities. *New J. Phys.* **15**, 025005, DOI: [10.1088/1367-2630/15/2/025005](https://doi.org/10.1088/1367-2630/15/2/025005) (2013).
5. Schlau-Cohen, G. S., Ishizaki, A. & Fleming, G. R. Two-dimensional electronic spectroscopy and photosynthesis: Fundamentals and applications to photosynthetic light-harvesting. *Chem. Phys.* **386**, 1–22, DOI: [10.1016/j.chemphys.2011.04.025](https://doi.org/10.1016/j.chemphys.2011.04.025) (2011).
6. Reppert, M. & Tokmakoff, A. Computational Amide I 2D IR Spectroscopy as a Probe of Protein Structure and Dynamics. *Annu. Rev. Phys. Chem.* **67**, 359–386, DOI: [10.1146/annurev-physchem-040215-112055](https://doi.org/10.1146/annurev-physchem-040215-112055) (2016).
7. Hume, S. *et al.* Measuring proteins in H₂O with 2D-IR spectroscopy. *Chem. Sci.* **10**, 6448–6456, DOI: [10.1039/c9sc01590f](https://doi.org/10.1039/c9sc01590f) (2019).
8. Thämer, M., De Marco, L., Ramasesha, K., Mandal, A. & Tokmakoff, A. Ultrafast 2D IR spectroscopy of the excess proton in liquid water. *Science* **350**, 78–82, DOI: [10.1126/science.aab3908](https://doi.org/10.1126/science.aab3908) (2015).
9. Bruder, L. *et al.* Coherent multidimensional spectroscopy of dilute gas-phase nanosystems. *Nat. Commun.* **9**, 4823, DOI: [10.1038/s41467-018-07292-w](https://doi.org/10.1038/s41467-018-07292-w) (2018). [1806.08314](https://doi.org/10.1038/s41467-018-07292-w).
10. Tiwari, V. *et al.* Spatially-resolved fluorescence-detected two-dimensional electronic spectroscopy probes varying excitonic structure in photosynthetic bacteria. *Nat. Commun.* **9**, 4219, DOI: [10.1038/s41467-018-06619-x](https://doi.org/10.1038/s41467-018-06619-x) (2018). [1802.04395](https://doi.org/10.1038/s41467-018-06619-x).
11. De Boeij, W. P., Pshenichnikov, M. S. & Wiersma, D. A. System-bath correlation function probed by conventional and time-gated stimulated photon echo. *J. Phys. Chem.* **100**, 11806–11823, DOI: [10.1021/jp961039m](https://doi.org/10.1021/jp961039m) (1996).
12. Everitt, K. F., Geva, E. & Skinner, J. L. Determining the solvation correlation function from three-pulse photon echoes in liquids. *J. Chem. Phys.* **114**, 1326–1335, DOI: [10.1063/1.1332811](https://doi.org/10.1063/1.1332811) (2001).
13. Gibson, E. A., Shen, Z. & Jimenez, R. Three-pulse photon echo peak shift spectroscopy as a probe of flexibility and conformational heterogeneity in protein folding. *Chem. Phys. Lett.* **473**, 330–335, DOI: [10.1016/j.cplett.2009.04.002](https://doi.org/10.1016/j.cplett.2009.04.002) (2009).
14. Mukamel, S. S. *Principles of nonlinear optical spectroscopy* (New York : Oxford University Press, 1995).
15. Yuen-Zhou, J. & Aspuru-Guzik, A. Quantum process tomography of excitonic dimers from two-dimensional electronic spectroscopy. I. General theory and application to homodimers. *J. Chem. Phys.* **134**, 134505, DOI: [10.1063/1.3569694](https://doi.org/10.1063/1.3569694) (2011).
16. Abramavicius, D., Butkus, V., Bujokas, J. & Valkunas, L. Manipulation of two-dimensional spectra of excitonically coupled molecules by narrow-bandwidth laser pulses. *Chem. Phys.* **372**, 22–32, DOI: [10.1016/j.chemphys.2010.04.015](https://doi.org/10.1016/j.chemphys.2010.04.015) (2010).
17. Collini, E. *et al.* Coherently wired light-harvesting in photosynthetic marine algae at ambient temperature. *Nature* **463**, 644–647, DOI: [10.1038/nature08811](https://doi.org/10.1038/nature08811) (2010).
18. Meneghin, E. *et al.* Coherence in carotenoid-to-chlorophyll energy transfer. *Nat. Commun.* **9**, 3160, DOI: [10.1038/s41467-018-05596-5](https://doi.org/10.1038/s41467-018-05596-5) (2018).
19. Paleček, D., Edlund, P., Westenhoff, S. & Zigmantas, D. Quantum coherence as a witness of vibronically hot energy transfer in bacterial reaction center. *Sci. Adv.* **3**, e1603141, DOI: [10.1126/sciadv.1603141](https://doi.org/10.1126/sciadv.1603141) (2017).
20. Scholes, G. D. *et al.* Using coherence to enhance function in chemical and biophysical systems. *Nature* **543**, 647–656 (2017).
21. Pan, J. *et al.* Ultrafast energy transfer within the photosystem II core complex. *Phys. Chem. Chem. Phys.* –, DOI: [10.1039/C7CP01673E](https://doi.org/10.1039/C7CP01673E) (2017).
22. Fuller, F. D. *et al.* Vibronic coherence in oxygenic photosynthesis. *Nat. Chem.* **6**, 706–711, DOI: [10.1038/nchem.2005](https://doi.org/10.1038/nchem.2005) (2014).
23. Lim, J. *et al.* Vibronic origin of long-lived coherence in an artificial molecular light harvester. *Nat. Commun.* **6**, 7755, DOI: [10.1038/ncomms8755](https://doi.org/10.1038/ncomms8755) (2015).
24. Thyryhaug, E. *et al.* Identification and characterization of diverse coherences in the Fenna - Matthews - Olson complex. *Nat. Chem.* **10**, 780–786, DOI: [10.1038/s41557-018-0060-5](https://doi.org/10.1038/s41557-018-0060-5) (2018).

25. Abramavicius, D. *et al.* Weak exciton scattering in molecular nanotubes revealed by double-quantum two-dimensional electronic spectroscopy. *Phys. Rev. Lett.* **108**, 067401, DOI: [10.1103/PhysRevLett.108.067401](https://doi.org/10.1103/PhysRevLett.108.067401) (2012).
26. Kim, J., Mukamel, S. & Scholes, G. D. Two-dimensional electronic double-quantum coherence spectroscopy. *Acc. Chem. Res.* **42**, 1375–1384, DOI: [10.1021/ar9000795](https://doi.org/10.1021/ar9000795) (2009).
27. Dostál, J. *et al.* Direct observation of exciton-exciton interactions. *Nat. Commun.* **9**, 2466, DOI: [10.1038/s41467-018-04884-4](https://doi.org/10.1038/s41467-018-04884-4) (2018).
28. Brüggemann, B. & Pullerits, T. Nonperturbative modeling of fifth-order coherent multidimensional spectroscopy in light harvesting antennas. *New J. Phys.* **13**, 025024, DOI: [10.1088/1367-2630/13/2/025024](https://doi.org/10.1088/1367-2630/13/2/025024) (2011).
29. Bubilaitis, V., Hauer, J. & Abramavicius, D. Simulations of pump probe spectra of a molecular complex at high excitation intensity. *Chem. Phys.* **527**, 110458, DOI: [10.1016/j.chemphys.2019.110458](https://doi.org/10.1016/j.chemphys.2019.110458) (2019).
30. Süß, J., Wehner, J., Dostál, J., Brixner, T. & Engel, V. Mapping of exciton - exciton annihilation in a molecular dimer via fifth-order femtosecond two-dimensional spectroscopy. *J. Chem. Phys.* **150**, 104304, DOI: [10.1063/1.5086151](https://doi.org/10.1063/1.5086151) (2019).
31. Fayer, M. D. (ed.) *Ultrafast Infrared Vibrational Spectroscopy* (CRC Press, 2013).
32. Remorino, A. & Hochstrasser, R. M. Three-dimensional structures by two-dimensional vibrational spectroscopy. *Acc. Chem. Res.* **45**, 1896–1905, DOI: [10.1021/ar3000025](https://doi.org/10.1021/ar3000025) (2012).
33. Smith, A. W. *et al.* Melting of β -hairpin peptide using isotope-edited 2D IR spectroscopy and simulations. *J. Phys. Chem. B* **114**, 10913–10924, DOI: [10.1021/jp104017h](https://doi.org/10.1021/jp104017h) (2010).
34. Anna, J. M., Baiz, C. R., Ross, M. R., McCanne, R. & Kubarych, K. J. Ultrafast equilibrium and non-equilibrium chemical reaction dynamics probed with multidimensional infrared spectroscopy. *Int. Rev. Phys. Chem.* **31**, 367–419, DOI: [10.1080/0144235X.2012.716610](https://doi.org/10.1080/0144235X.2012.716610) (2012).
35. Fayer, M. D. *et al.* Water dynamics in salt solutions studied with ultrafast two-dimensional infrared (2D IR) vibrational echo spectroscopy. *Acc. Chem. Res.* **42**, 1210–1219, DOI: [10.1021/ar900043h](https://doi.org/10.1021/ar900043h) (2009).
36. Ji, M., Park, S. & Gaffney, K. J. Dynamics of ion assembly in solution: 2DIR spectroscopy study of LiNCS in benzonitrile. *J. Phys. Chem. Lett.* **1**, 1771–1775, DOI: [10.1021/jz100486x](https://doi.org/10.1021/jz100486x) (2010).
37. Ng Pack, G. *et al.* Two-dimensional infrared spectroscopy from the gas to liquid phase: Density dependent: J -scrambling, vibrational relaxation, and the onset of liquid character. *Phys. Chem. Chem. Phys.* **21**, 21249–21261, DOI: [10.1039/c9cp04101j](https://doi.org/10.1039/c9cp04101j) (2019).
38. Cyran, J. D., Nite, J. M. & Krummel, A. T. Characterizing Anharmonic Vibrational Modes of Quinones with Two-Dimensional Infrared Spectroscopy. *J. Phys. Chem. B* **119**, 8917–8925, DOI: [10.1021/jp506900n](https://doi.org/10.1021/jp506900n) (2015).
39. Guo, Q., Pagano, P., Li, Y. L., Kohen, A. & Cheatum, C. M. Line shape analysis of two-dimensional infrared spectra. *J. Chem. Phys.* **142**, 212427, DOI: [10.1063/1.4918350](https://doi.org/10.1063/1.4918350) (2015).
40. Laane, J. Vibrational Potential Energy Surfaces in Electronic Excited States. In *Front. Mol. Spectrosc.*, 63–132, DOI: [10.1016/B978-0-444-53175-9.00004-0](https://doi.org/10.1016/B978-0-444-53175-9.00004-0) (Elsevier, 2009).
41. Laane, J. Experimental determination of vibrational potential energy surfaces and molecular structures in electronic excited states. *J. Phys. Chem. A* **104**, 7715–7733, DOI: [10.1021/jp0009002](https://doi.org/10.1021/jp0009002) (2000).
42. Chen, J., Sun, Z. & Zhang, D. H. An accurate potential energy surface for the F + H₂ → HF + H reaction by the coupled-cluster method. *J. Chem. Phys.* **142**, 024303, DOI: [10.1063/1.4904546](https://doi.org/10.1063/1.4904546) (2015).
43. Knochenmuss, R., Sinha, R. K. & Leutwyler, S. Intermolecular dissociation energies of dispersively bound complexes of aromatics with noble gases and nitrogen. *J. Chem. Phys.* **148**, 134302, DOI: [10.1063/1.5019432](https://doi.org/10.1063/1.5019432) (2018).
44. Zúñiga, J., Picón, J. A., Bastida, A. & Requena, A. A spectroscopic potential energy surface for FCN. *J. Quant. Spectrosc. Radiat. Transf.* **113**, 1155–1169, DOI: [10.1016/j.jqsrt.2012.01.023](https://doi.org/10.1016/j.jqsrt.2012.01.023) (2012).
45. Dong, W. *et al.* Transition-state spectroscopy of partial wave resonances in the F + HD reaction. *Science* **327**, 1501–1502, DOI: [10.1126/science.1185694](https://doi.org/10.1126/science.1185694) (2010).
46. Yan, Z., Gray, S. K. & Scherer, N. F. Potential energy surfaces and reaction pathways for light-mediated self-organization of metal nanoparticle clusters. *Nat. Commun.* **5**, DOI: [10.1038/ncomms4751](https://doi.org/10.1038/ncomms4751) (2014).
47. Skúlason, E. *et al.* Modeling the electrochemical hydrogen oxidation and evolution reactions on the basis of density functional theory calculations. *J. Phys. Chem. C* **114**, 18182–18197, DOI: [10.1021/jp1048887](https://doi.org/10.1021/jp1048887) (2010).

48. Pechukas, P. Transition State Theory. *Annu. Rev. Phys. Chem.* **32**, 159–177, DOI: [10.1146/annurev.pc.32.100181.001111](https://doi.org/10.1146/annurev.pc.32.100181.001111) (1981).
49. Satzger, H., Root, C. & Braun, M. Excited-state dynamics of trans- and cis-azobenzene after UV excitation in the $\pi\pi^*$ band. *J. Phys. Chem. A* **108**, 6265–6271, DOI: [10.1021/jp049509x](https://doi.org/10.1021/jp049509x) (2004).
50. Johnson, P. J. *et al.* Local vibrational coherences drive the primary photochemistry of vision. *Nat. Chem.* **7**, 980–986, DOI: [10.1038/nchem.2398](https://doi.org/10.1038/nchem.2398) (2015).
51. Balevičius, V. *et al.* The full dynamics of energy relaxation in large organic molecules: From photo-excitation to solvent heating. *Chem. Sci.* **10**, 4792–4804, DOI: [10.1039/c9sc00410f](https://doi.org/10.1039/c9sc00410f) (2019).
52. Hauer, J. *et al.* Explaining the temperature dependence of Spirilloxanthin's S* signal by an inhomogeneous ground state model. *J. Phys. Chem. A* **117**, 6303–6310, DOI: [10.1021/jp4011372](https://doi.org/10.1021/jp4011372) (2013).
53. Jambrina, P. G., González-Sánchez, L., Aldegunde, J., Saéz-Rábanos, V. & Aoiz, F. J. Competing Dynamical Mechanisms in Inelastic Collisions of H + HF. *J. Phys. Chem. A* **123**, 9079–9088, DOI: [10.1021/acs.jpca.9b07272](https://doi.org/10.1021/acs.jpca.9b07272) (2019).
54. Sáez-Rábanos, V., Verdasco, J. E. & Herrero, V. J. Orbiting resonances in the F + HD (: V = 0, 1) reaction at very low collision energies. A quantum dynamical study. *Phys. Chem. Chem. Phys.* **21**, 15177–15186, DOI: [10.1039/c9cp02718a](https://doi.org/10.1039/c9cp02718a) (2019).
55. Le Roy, R. J., Huang, Y. & Jary, C. An accurate analytic potential function for ground-state N₂ from a direct-potential-fit analysis of spectroscopic data. *J. Chem. Phys.* **125**, 164310, DOI: [10.1063/1.2354502](https://doi.org/10.1063/1.2354502) (2006).
56. de Lima, E. F. & Hornos, J. E. M. Matrix elements for the Morse potential under an external field. *J. Phys. B At. Mol. Opt. Phys.* **38**, 815–825, DOI: [10.1088/0953-4075/38/7/004](https://doi.org/10.1088/0953-4075/38/7/004) (2005).
57. Borek, J. A., Perakis, F. & Hamm, P. Testing for memory-free spectroscopic coordinates by 3D IR exchange spectroscopy. *Proc. Natl. Acad. Sci.* **111**, 10462–10467, DOI: [10.1073/pnas.1406967111](https://doi.org/10.1073/pnas.1406967111) (2014).
58. Fidler, A. F., Harel, E. & Engel, G. S. Dissecting Hidden Couplings Using Fifth-Order Three-Dimensional Electronic Spectroscopy. *J. Phys. Chem. Lett.* **1**, 2876–2880, DOI: [10.1021/jz101064j](https://doi.org/10.1021/jz101064j) (2010).
59. Zhang, Z., Lambrev, P. H., Wells, K. L., Garab, G. & Tan, H.-S. Direct observation of multistep energy transfer in LHCII with fifth-order 3D electronic spectroscopy. *Nat. Commun.* **6**, 7914, DOI: [10.1038/ncomms8914](https://doi.org/10.1038/ncomms8914) (2015).
60. Li, H., Bristow, A. D., Siemens, M. E., Moody, G. & Cundiff, S. T. Unraveling quantum pathways using optical 3D Fourier-transform spectroscopy. *Nat. Commun.* **4**, 1390, DOI: [10.1038/ncomms2405](https://doi.org/10.1038/ncomms2405) (2013).
61. Mueller, S. *et al.* Rapid multiple-quantum three-dimensional fluorescence spectroscopy disentangles quantum pathways. *Nat. Commun.* **10**, 4735, DOI: [10.1038/s41467-019-12602-x](https://doi.org/10.1038/s41467-019-12602-x) (2019).
62. Turner, D. B. & Nelson, K. A. Coherent measurements of high-order electronic correlations in quantum wells. *Nature* **466**, 1089–1092, DOI: [10.1038/nature09286](https://doi.org/10.1038/nature09286) (2010).
63. Valkunas, L., Abramavicius, D. & Mancal, T. *Molecular Excitation Dynamics and Relaxation: Quantum Theory and Spectroscopy* (Wiley-VCH Verlag GmbH & Co. KGaA, Weinheim, Germany, 2013).
64. Tanimura, Y. The 5th- and 7th-order 2D Raman spectroscopy for intramolecular vibrational modes. In *AIP Conf. Proc.*, vol. 503, 144–153, DOI: [10.1063/1.1302858](https://doi.org/10.1063/1.1302858) (AIP, 2000).
65. Kubarych, K. J., Milne, C. J. & Miller, R. J. D. Fifth-order two-dimensional Raman spectroscopy: A new direct probe of the liquid state. *Int. Rev. Phys. Chem.* **22**, 497–532, DOI: [10.1080/0144235031000121544](https://doi.org/10.1080/0144235031000121544) (2003).
66. Molesky, B. P., Giokas, P. G., Guo, Z. & Moran, A. M. Multidimensional resonance raman spectroscopy by six-wave mixing in the deep UV. *J. Chem. Phys.* **141**, 114202, DOI: [10.1063/1.4894846](https://doi.org/10.1063/1.4894846) (2014).
67. Molesky, B. P., Guo, Z. & Moran, A. M. Femtosecond stimulated Raman spectroscopy by six-wave mixing. *J. Chem. Phys.* **142**, 212405, DOI: [10.1063/1.4914095](https://doi.org/10.1063/1.4914095) (2015).
68. Kirkwood, J. C. & Albrecht, A. C. Multi-dimensional time-resolved coherent Raman six-wave mixing: a comparison of the direct and cascaded processes with femtosecond excitation and noisy light interferometry. *J. Raman Spectrosc.* **31**, 107–124, DOI: [10.1002/\(SICI\)1097-4555\(200001/02\)31:1/2<107::AID-JRS493>3.0.CO;2-E](https://doi.org/10.1002/(SICI)1097-4555(200001/02)31:1/2<107::AID-JRS493>3.0.CO;2-E) (2000).
69. Cho, M. *et al.* Intrinsic cascading contributions to the fifth- and seventh-order electronically off-resonant Raman spectroscopies. *J. Chem. Phys.* **112**, 2082–2094, DOI: [10.1063/1.480777](https://doi.org/10.1063/1.480777) (2000).
70. Mehlenbacher, R. D., Lyons, B., Wilson, K. C., Du, Y. & McCamant, D. W. Theoretical analysis of anharmonic coupling and cascading Raman signals observed with femtosecond stimulated Raman spectroscopy. *J. Chem. Phys.* **131**, 244512, DOI: [10.1063/1.3276684](https://doi.org/10.1063/1.3276684) (2009).

71. Spencer, A. P., Hutson, W. O. & Harel, E. Quantum coherence selective 2D Raman–2D electronic spectroscopy. *Nat. Commun.* **8**, 14732, DOI: [10.1038/ncomms14732](https://doi.org/10.1038/ncomms14732) (2017).

Acknowledgements

The author acknowledges financial support of Lithuanian Science Council (grant No: SMIP-20-47)